OPEN ACCESS
IOP Publishing
Journal of Physics D: Applied Physics
J. Phys. D: Appl. Phys. **55** (2022) 395204 (10pp)
https://doi.org/10.1088/1361-6463/ac7fc6

Development of a microkinetic model for non-oxidative coupling of methane over a Cu catalyst in a non-thermal plasma reactor

Nima Pourali[1,*], Maksim Vasilev[2], Rufat Abiev[2] and Evgeny V Rebrov[1,2,*]

[1] School of Engineering, University of Warwick, Coventry CV4 7AL, United Kingdom
[2] Department of Optimization of Chemical and Biotechnological Equipment, Saint-Petersburg State Institute of Technology (Technical University), Saint-Petersburg 190013, Russia

E-mail: n.pourali86@gmail.com and e.rebrov@warwick.ac.uk

Received 20 April 2022, revised 14 June 2022
Accepted for publication 8 July 2022
Published 22 July 2022

Abstract

A surface microkinetic plasma model for non-oxidative coupling of methane into H_2 and higher hydrocarbons was developed over a Cu catalytic film. Twenty key plasma species including electron, ions, radicals, and neutrals were considered in respective chemical reactions leading to the formation of C2 hydrocarbons onto the catalyst surface. The kinetic model was coupled with a global plasma model to describe the performance of a non-thermal plasma reactor. In the reactor model, the reactant gas flows between the two coaxial cylindrical metal electrodes with a length of 50 mm and a diameter of 2 mm (inner) and 6 mm (outer electrode) coated with a Cu film. The effect of discharge power, initial CH_4 concentration, and inlet flow rate on methane conversion was investigated. The surface model shows that the CH_4 conversion of 47% is obtained at a discharge power of 70 W with a selectivity of C_2H_2 (49%). Increase in power increased the conversion of methane while increase in pressure and/or inlet gas flow rate decreased it. Also, the results of the plasma-catalyst model were compared with those of plasma alone (without catalyst). It showed that presence of the catalyst inside the plasma increases the selectivity and yield of acetylene, while it deceases the selectivity and yield of hydrogen. Also, the density of radical CH_3 in the plasma phase increased in the presence of catalyst, while CH_2 and CH densities decreased with that.

Keywords: non-oxidative methane coupling, microkinetic surface model, non-thermal plasma

(Some figures may appear in colour only in the online journal)

* Authors to whom any correspondence should be addressed.

1. Introduction

The growing energy demand together with decreasing reserves of oil have accentuated the need to develop alternative processes for making fuels and chemicals. Methane is the main component of natural gas and biogas therefore its conversion into hydrogen and value-added chemicals such as C_2H_2, C_2H_4, and C_3H_6 has attracted great interest. A conventional thermal catalytic process approach to convert methane to higher hydrocarbons requires high temperatures (>700 °C) and use of catalysts to facilitate this process. The deposition of carbon layers onto the catalyst surface leads to the fast catalyst deactivation, especially for supported non-noble metal catalysts resulting in high regeneration costs [1–3]. Therefore, developing alternative methods and processes for direct conversion of methane to higher hydrocarbons has attracted a lot of attention.

Non-thermal plasma (NTP) offers an attractive alternative to the conventional catalytic route for the CH_4 conversion at atmospheric pressure and relatively low temperatures which can inhibit carbon deposition [4–8]. The overall gas temperature can be as low as room temperature, while the electron temperatures of 10 eV can easily break down methane molecules and produce a variety of species: free radicals, excited atoms and ions [9]. Further coupling and chain propagation reactions within the plasma lead to the formation of higher hydrocarbons. Thus, NTP could enable thermodynamically unfavorable reactions to occur under ambient conditions.

Considerable amount of research has been performed to investigate the effectiveness of CH_4 conversion by using dielectric barrier discharge (DBD) plasma. A potential method to improve the selectivity of the process is to place a catalyst into the plasma zone close to the electrode [10–12]. The catalyst could accelerate the reaction rates of specific pathways to increase the selectivity towards desirable hydrocarbons. The catalyst could also provide new reaction pathways in addition to those occurring in the discharge volume. The strong electric filed could lower the activation barrier of surface processes, and modify the reaction kinetics [12].

Catalytic plasma processing of methane is a rather complex process and a fundamental understanding of the underlying physical phenomena and chemical reactions onto the catalyst surface is still very limited, making it difficult to optimize processing parameters and predict the conversion and selectivity of products theoretically. This is partially due to the complexity of the related calculations as well as lack of underlying kinetic data. In fact, the absence of reliable data on elementary steps remains a limiting factor. Also, high computing power is required due to the coupling of the transport equations in the reactor volume with the surface equations on the catalyst surface. While numerical techniques and computing power have been advanced over the last decades, efficient multi-dimensional modeling of plasma assisted catalytic reactors still represents a considerable challenge. However, development of plasma-catalytic models is crucial for the rational design of novel plasma reactors and optimization of highly complex plasma processes. Because the modeling of the plasma assisted catalytic reactor requires, in addition to a plasma model, employing a microkinetic surface model to incorporate all the essential surface steps occurring onto the catalyst surface. Microkinetic modeling of methane plasma chemistry was already applied to predict the reaction rates and product distribution in the plasma assisted synthesis of carbon nanotubes onto the catalyst surface [13–15]. A microkinetic model was proposed for the synthesis of carbon shells in acetylene plasma. The model included the steps of nanofibers growth, the restructuring of catalyst particles, and the formation of the carbon layer on the catalyst surface [13, 14]. A theoretical model was also proposed to calculate the particle density and the growth kinetics [15]. The latter described the rates of species deposition reactions onto the catalyst surface, as well as the kinetics of neutrals, ionic particles and electrons, and the rate of charge accumulation on the surface.

Using a gradientless reactor model (a so-called global model (GM) in terms of plasma description) requires considerably lower computational time and permits one to investigate the plasma and gas chemical kinetics for the species present in the discharge and to study effect of operating conditions such as gas temperature, gas flow rate, and discharge power on plasma properties [16–19]. The main disadvantage of the GM is that the discharge structure and the plasma dynamics cannot be described [20, 21].

In this study, the plasma non-oxidative conversion of CH_4 into hydrogen and higher hydrocarbons has been investigated in a DBD reactor over a Cu catalyst under ambient conditions. The copper catalysts promote coupling reactions at rather high rates at ambient temperature [22]. To the best of our knowledge, no previous studies were devoted to the coupling of a microkinetic surface model with a plasma model to describe the reaction of plasma assisted non-oxidative coupling of methane. Although the effects of plasma on catalyst reaction mechanisms have been recently reported in some papers [12, 23], this work is the first attempt at the coupling plasma model with the surface micro-kinetic model. In the previous works, the densities of species in the plasma phase were assumed to constant and there was no time evolution for them during the process. Here, a simplified microkinetic model that includes 22 surface reaction steps was used. The transition state theory was employed to estimate the rates of forward and backward surface reactions. The activation energies and the rates of individual surface steps were obtained from the density function theory (DFT) CatApp database [24]. Then the surface kinetic model was combined with a plasma reactor model, which consists of 30 volumetric reactions and convective mass transport of reactive species. The possible reaction mechanisms leading to the formation of major gas products and their selectivity are discussed.

2. Description of the model

2.1. GM of methane plasma

In this section, we describe a plasma GM that developed by ourself for studying the chemistry of atmospheric-pressure methane plasma formed inside a cylindrical DBD. The plasma reactor is formed by two coaxial cylindrical electrodes with

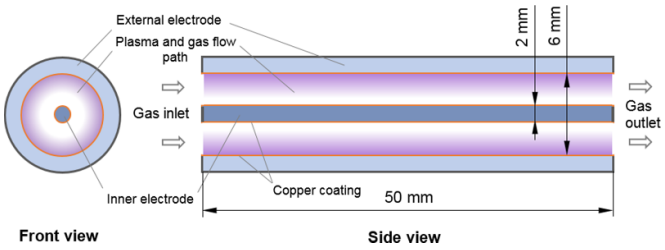

Figure 1. Scheme of coaxial plasma reactor used in this work.

Table 1. Species considered in bulk methane plasma.

No.	Species	No.	Species	No.	Species	No.	Species
1	H	6	CH_4	11	C_2H_6	16	CH_4^+
2	H_2	7	C_2H_2	12	C_3H_5	17	CH_5^+
3	CH	8	C_2H_3	13	C_3H_6	18	$C_2H_2^+$
4	CH_2	9	C_2H_4	14	C_3H_8	19	$C_2H_5^+$
5	CH_3	10	C_2H_5	15	CH_3^+	20	e

a length of 50 mm and a diameter of 2 mm and 6 mm. The two ends of cylinders are open to the flow (figure 1). A copper coating covers the walls of both cylinders. The global plasma model describes a plasma discharge volume ($V_{\rm dis}$) that is enclosed by the surface area ($A_{\rm wall}$). It is assumed that plasma is spatially uniform and the power is absorbed uniformly into the discharge. The model considered here is well known as the global or zero-dimensional model. The GM is a volume-averaged fluid model, with great advantages in speed and simplicity. This model is based on two types of the equation: particle balance equations, written for each included species, and power balance equations, which are primarily used for electrons, but can be included for other species. Also, in this model any species and energy added to and removed from bulk plasma due to reactor inlet and outlet as well as surfaces reactions are taken into account in balance equations. The Maxwellian energy distribution function is considered for heavy species (neutrals and ions) [18, 25]. In atmospheric NTPs, due to low ionization degree and high collision rate, ions are in thermal balance with neutral species and background gas, which have comparable mass with ions. Therefore, in this work, it is assumed that heavy species have the same and constant temperature and they are in thermal balance with each other. The latter suggests that ions and neural species have Maxwellian distribution. Twenty key plasma species including electron, ions, radicals, and neutrals are assumed to take part in chemical reactions. They are listed in table 1.

The plasma phase reactions taking place in the bulk plasma are listed in table II in our previous work [26]. The rate constants of the interaction of the electron with background gases and neutral species have been taken from look-up tables constructed by a Boltzmann equation solver following the approach presented in [27]. To construct the look-up table that gives electron rate constants as a function of the electron mean energy, in this work we used BOLSING+ (see www.lxcat.laplace.univ-tlse.fr for a website to access BOLSIG+, which is a free software for the numerical solution of the Boltzmann equation for electrons in weakly ionized gases). This website also includes electron-impact cross-sections of the different commonly used gases in plasma processing. This software calculates the transport coefficient, the rate constant and electron mean energy for each value of E/N. It is obvious that with having electron mean energy and rate constants for different E/N, one can construct a table that gives rate constants versus electron mean energy. It is worthwhile to mention that this offline software itself calculates the transport coefficient and rate constants versus mean electron energy too. In this software rate coefficients are calculated from collision cross-section data by solving the electron Boltzmann equation (two-term approximation). It means that cross-section data for each reaction is inserted as an input parameter. The rate constants of ion-neutral and neutral-neutral reactions have been taken from [28–33]. Equation (1) is the balance equation for number density of ions and neutrals (n_j) [19, 34, 35].

$$\frac{\partial n_j}{\partial t} = F_{\rm flow\_in,j} - F_{\rm flow\_out,j} + \omega_{\rm reac,j} - \frac{S\Gamma_{s,j}}{V_{\rm dis}} \tag{1}$$

where $F_{\rm flow\_in,j}$ is the inlet flow rate, $F_{\rm flow\_out,j}$ is the outlet flow rate, $\omega_{\rm reac,j}$ is the bulk reaction source term and $S\Gamma_{s,j}/V_{\rm dis}$ is the surface consumption term [36–39]. The outlet flow rate is a function of reaction stoichiometry and in general it does not equal to the inlet flow rate as the reactor operates at a constant pressure. The reaction source term for each species is calculated by equation (2) [18]

$$\omega_{\rm reac,j} = \sum_k \left(a_{jk}^R - a_{jk}^L\right) k_k \prod_l n_l^L \tag{2}$$

where a_{jk}^R and a_{jk}^L are the right-hand side and left-hand side stoichiometric coefficients of species j in reaction k, k_k is the reaction rate coefficient and n_l^L is the number density of the lth species in the left-hand side of reaction k. Flux into the boundary, $\Gamma_{s,j}$, is given by

$$\Gamma_{s,j} = \gamma_j n_j v_{{\rm th},j}, \tag{3}$$

where $v_{{\rm th},j}$ is the thermal velocity ($v_{{\rm th},j} = \sqrt{8k_BT_j/\pi m_j}$) with k_B, T_j, and m_j being the Boltzmann constant, species temperature, and species mass, respectively. The coefficient γ_j in equation (3) for neutral species is the effective sticking coefficient which is self-consistently determined by the surface kinetic model. The sticking probability of ions on the catalyst surface is 1. The γ_j for ions is equal to 0.25. The latter is determined by Maxwellian directed flux near the surface (see equation (2.4.10) in the [40]). The total pressure, $P_{\rm tot}$, in the discharge is assumed to obey the ideal gas law:

$$p_{\rm tot} = k_B T_g \sum_n n_n. \tag{4}$$

The number density of electron in discharge center is determined from the charge neutrality equation:

$$n_e = \sum_i n_i \tag{5}$$

Table 2. Kinetic parameters for adsorption/desorption reactions on a Cu (211) surface.

No.	Reaction	E_{ads} (eV)	E_{des} (eV)	Reference
RS1	$H_{(plasma)} + [\,] \leftrightarrow H_{(ads)}$	0.0	2.4	[41]
RS2	$H_{2(plasma)} + [\,] \leftrightarrow H_{2(ads)}$	0.0	0.68	[42]
RS3	$CH_{(plasma)} + [\,] \leftrightarrow CH_{(ads)}$	0.0	5.58	[42]
RS4	$CH_{2(plasma)} + [\,] \leftrightarrow CH_{2(ads)}$	0.0	3.4	[42]
RS5	$CH_{3(plasma)} + [\,] \leftrightarrow CH_{3(ads)}$	0.0	1.4	[42]
RS6	$CH_{4(plasma)} + [\,] \leftrightarrow CH_{4(ads)}$	0.0	0.13	[42]
RS7	$C_2H_{2(plasma)} + [\,] \leftrightarrow C_2H_{2(ads)}$	0.0	0.1	[12]
RS8	$C_2H_{3(plasma)} + [\,] \leftrightarrow C_2H_{3(ads)}$	0.0	1.46	[12]
RS9	$C_2H_{4(plasma)} + [\,] \leftrightarrow C_2H_{4(ads)}$	0.04	0.0	[43]
RS10	$C_2H_{5(plasma)} + [\,] \leftrightarrow C_2H_{5(ads)}$	0.0	1.35	[12]
RS11	$C_2H_{6(plasma)} + [\,] \leftrightarrow C_2H_{6(ads)}$	0.0	0.0	[44]

Table 3. Kinetic parameters for surface reactions on a Cu (211) surface.

No.	Reaction	E_f (eV)	E_b (eV)	Reference
RS12	$H_{2(ads)} + [\,] \leftrightarrow 2H_{(ads)}$	0.78	0.63	[47]
RS13	$CH_{4(ads)} + [\,] \leftrightarrow CH_{3(ads)} + H_{(ads)}$	0.7	1.9	[43]
RS14	$CH_{(ads)} + H_{(ads)} \leftrightarrow CH_{2(ads)} + [\,]$	0.79	1.2	[43]
RS15	$CH_{2(ads)} + H_{(ads)} \leftrightarrow CH_{3(ads)} + [\,]$	0.64	1.6	[43]
RS16	$C_2H_{2(ads)} + H_{(ads)} \leftrightarrow C_2H_{3(ads)} + [\,]$	1.29	1.58	[48]
RS17	$C_2H_{3(ads)} + H_{(ads)} \leftrightarrow C_2H_{4(ads)} + [\,]$	0.5	1.9	[43]
RS18	$C_2H_{4(ads)} + H_{(ads)} \leftrightarrow C_2H_{5(ads)} + [\,]$	0.59	0.89	[43]
RS19	$C_2H_{5(ads)} + H_{(ads)} \leftrightarrow C_2H_{6(ads)} + [\,]$	0.6	1.7	[43]
RS20	$2CH_{(ads)} \leftrightarrow C_2H_{2(ads)} + [\,]$	0.7	2.0	[44]
RS21	$2CH_{2(ads)} \leftrightarrow C_2H_{4(ads)} + [\,]$	0.0	2.2	[44]
RS22	$2CH_{3(ads)} \leftrightarrow C_2H_{6(ads)} + [\,]$	1.9	3.0	[44]

The electron temperature is calculated from the power balance equation [18, 49, 50]

$$\frac{\partial\left(\frac{3}{2}k_B T_e n_e\right)}{\partial t} = \frac{P_{abs}}{V_{dis}} - (P_{en} + P_s) \tag{6}$$

where P_{abs} is the discharge power, P_{en} is the electron power loss due to all electron-neutral collision processes, and P_s is the charged particle total power losses to reactor walls. The latter two terms are calculated by equations (7) and (8), respectively.

$$P_{en} = \sum_n \left(\frac{3m_e}{m_n} k_B T_e\right) k_{el,n} n_e n_n + \sum_n E_{th,n} k_n n_e n_n \tag{7}$$

$$P_s = \left(\frac{S}{V_{dis}}\right)\left(\Gamma_{s,e} E_{es} + \sum_i \Gamma_{s,i} E_{is}\right) \tag{8}$$

where T_e is electron temperature, m_e is electron mass, m_n is mass of neutral n, $E_{th,n}$ is the activation energy for the reactions n that electron participate in, and $k_{el,n}$ and k_n, respectively, are the rate coefficient for elastic and inelastic collisions of electron with neutral species n. E_{es} and E_{is} denote the mean kinetic energy per particle of the electrons and ions reaching the surfaces, respectively.

2.2. Microkinetic model on a Cu catalyst

The species produced in the plasma absorbed onto the catalyst surface and participate in surface reactions similar to conventional catalysis. Based on preliminary sensitivity analysis, 11 key species have been selected for the development of the surface microkinetic model. The surface reaction mechanism includes 22 elementary steps that can be split up into two main groups. The first group contains 11 reversible adsorption steps (RS1–RS11, table 2), while the second group contains 11 surface reaction steps (RS12–RS22, table 3). Where [] symbolizes an adsorption site on the catalyst, and A* is an adsorbate attached to one of these sites. Following the classical adsorption theory, the adsorption rate is proportional to the empty coverage sites

$$r_{ads,j} = A_{st}\left(1 - \sum_j \theta_j\right)\left(n_j \nu_{th,j}\right), \tag{9}$$

where θ_j is the surface coverages of species j, n_j is the density of species j, and A_{st} is the pre-exponential factor of adsorption. The desorption rate is proportional to the coverage with species j

$$r_{des,j} = \theta_j \frac{k_B T_s}{h} \exp\left(-\frac{E_{des}}{k_B T_s}\right), \tag{10}$$

where h is the Planck's constant, E_{des} is the desorption activation energy, and T_s is the surface temperature. For the reversible surface reactions with adsorbed species $A_{(ads)}$, $B_{(ads)}$, and $C_{(ads)}$:

$$A_{(ads)} + B_{(ads)} \leftrightarrow C_{(ads)} + [\,], \tag{11}$$

the harmonic transition state theory [44] is used to obtain the forward and backward rate constants

$$k_f = \frac{k_B T_s}{h} \frac{q^{\ddagger}_{\text{vib}}}{q^{A}_{\text{vib}} q^{B}_{\text{vib}}} \exp\left(-\frac{E_f}{k_B T_s}\right), \tag{12}$$

$$k_b = \frac{k_B T_s}{h} \frac{q^{\ddagger}_{\text{vib}}}{q^{C}_{\text{vib}}} \exp\left(-\frac{E_b}{k_B T_s}\right), \tag{13}$$

where, $q^{\ddagger}_{\text{vib}}$, q^{A}_{vib}, q^{B}_{vib}, and q^{C}_{vib} are the vibrational partition functions for the transition state and E_f and E_b are the activation energy for the forward and backward reactions, respectively. The activation energies were taken from the CatApp database [24]. It is worth noting that surface species often have no translational or rotational degrees of freedom, so the pre-exponential factors are calculated based on vibrational degrees of freedom [45]. The vibrational partition function is defined as the product of the contribution of each vibrational mode,

$$q_{\text{vib}} = \prod_{l} \frac{1}{1 - \exp\left(\frac{-h\nu_l}{k_B T_l}\right)}, \tag{14}$$

where ν_l is the frequency of the corresponding vibration mode of the molecule [46]. The number of vibrational modes of a non-linear molecule containing n atoms is equal to $3n-5$. It is assumed that the geometry of the transition state corresponds to the geometry of the product for all surface reactions described by equation (11). Therefore, the vibrational partition function of the transition state is replaced with vibrational partition function of the product, i.e. $q^{\ddagger}_{\text{vib}} = q^{C}_{\text{vib}}$. Having rate constants of each surface reaction, the balance equation for surface species j can be written in following form

$$\frac{\partial \theta_j}{\partial t} = r_{\text{ads},j} - r_{\text{des},j} + \sum_i a_{ij} r_i, \tag{15}$$

with

$$r_i = k_{fi} \prod_j \theta_j^{a_{ij}} - k_{bi} \prod_j \theta_j^{a_{ij}} \tag{16}$$

where a_{ij} is the stoichiometric coefficient of species j in surface reaction i. Notice, the summation in equation (15) counts surface reactions RS12–RS22 only. The solution of equation (15) provides the surface coverage for all surface species (θ_j) and the respective reaction rates of all surface steps. Finally, the effective sticking coefficients, γ_n, for each gas phase species is calculated by following relation (3),

$$\gamma_n = \frac{(r_{\text{ads},n} - r_{\text{des},n})}{A_{\text{st}} n_n v_{\text{th}}} n = 1, 2, \ldots \tag{17}$$

The solution of surface reaction model needs a value of gas phase densities which are calculated in the global plasma model. On the other hand, the GM uses the effective sticking coefficients as input parameter to calculate the gas phase densities. This implies that the plasma and surface kinetic models are coupled and equations (1) and (15) must be solved simultaneously. A Fortran code was developed to solve these coupled equations. Explicit Euler method was used to solve ordinary differential equations in plasma model while fourth order Rang Kutta approach was employed to solve balance equations in surface microkinetic model. Time step in plasma model was chosen to be 1.0×10^{-11} s while for surface microkinetic model the time step set to 1.0×10^{-13} s. The later implies that the surface model run 100 times in each plasma time step. In each plasma time step, the surface model must be in its steady state. Therefore, we need to choose a smaller time step for the surface model to be sure that it reaches to steady state before the next plasma time step starts. The effects of total pressure, reaction time and the discharge power were studied. The other parameters were fixed (see table 4). The output parameters were the plasma density, the concentrations of gas species and the electron energy. The CH_4 conversion (X), the product yield (Y) and the selectivity towards key products (S) are calculated from the species density.

Table 4. Process parameters.

Parameter	Value
Inlet gas temperature, T_g	300 K
Inlet flow rate, $F_{\text{flow\_in},j}$	30–90 ml cm^{-3} (STP)
Discharge power, P_{abs}	50–90 W
Surface temperature, T_s	300 K
Reactor pressure, p	0.8–1.2 atm
Plasma discharge volume, V_{dis}	1.26 cm^3
External wall surface area, A_{wall}	12.6 cm^2

$$X_{CH_4}(\%) = \frac{n_{CH_4,\text{converted}}}{n_{CH_4,\text{in}}} \times 100, \tag{18}$$

$$Y_{H_2}(\%) = \frac{n_{H_2}}{2 \times n_{CH_4,\text{in}}} \times 100, \tag{19}$$

$$Y_{C_xH_y}(\%) = \frac{x \times n_{C_xH_y}}{n_{CH_4,\text{in}}} \times 100, \tag{20}$$

$$S_{H_2}(\%) = \frac{n_{H_2}}{2 \times n_{CH_4,\text{converted}}} \times 100, \tag{21}$$

$$S_{C_xH_y}(\%) = \frac{x \times n_{C_xH_y}}{n_{CH_4,\text{converted}}} \times 100. \tag{22}$$

3. Results and discussion

This section presents the results obtained from kinetic model described in previous section. Before coupling the plasma model to the micro-kinetic surface model, a global plasma model with a consistent set of 367 gas-phase reactions and the 36 defined species, describing complete methane plasma chemistry was used to make a reduced chemistry mechanism. This model without surface microkinetic model was run in different plasma conditions (pressures, powers, flows). After each run, species with higher densities were selected and the main reactions producing and consuming these species were

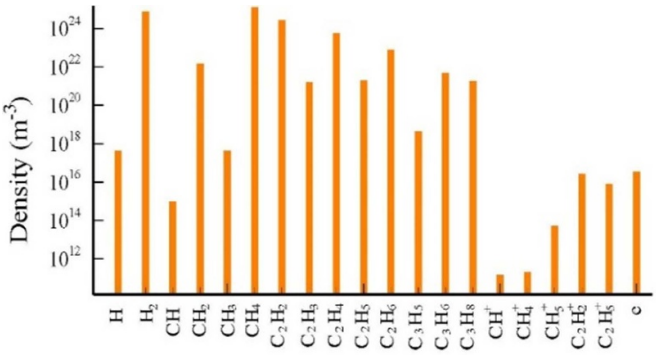

Figure 2. The steady state concentrations of key plasma species at inlet gas temperature: 300 K, surface temperature: 300 K, discharge power: 70 W, flow rate: 50 ml min^{-1}, and pressure: 1.0 atm.

determined. The results of different conditions were compared with each other. Finally, 20 species with 30 main reactions were selected to make a reduced chemistry mechanism that represents the whole methane plasma chemistry and requires a lower computational cost. In the case of surface chemistry mechanism, considered reactions are the same as those in [12]. The surface reaction mechanism considered here contains all possible surface processes and reactions that take place on the surface of Cu catalyst immersed in the methane plasma environment. Activation barrier and reaction energy for each reaction were used form DFT database [24].

The steady-state concentrations of key reactive species at a discharge power of 70 W and a gas flow rate of 50 ml min^{-1} are shown in figure 2. It can be seen that hydrogen, acetylene and ethylene are the main reaction products. The concentrations of ethane, propene and propane are almost two orders of magnitude lower. Therefore, the subsequent discussion will be focused on the three main products only.

Figure 3(a) shows that a methane conversion of 47% was achieved after a discharge time of 2 s. The final yield of hydrogen (15%) is lower than that of acetylene (23%). The ethylene yield was about 4.1%. The selectivity for both acetylene and hydrogen increase with CH_4 conversion while the ethylene selectivity decreases with that (see figure 3(b)). When the surface model is coupled with the plasma model the whole chemistry describing the conversion process becomes more complicated and tracing reaction pathways leading to the production and consumption of species is more challenging. Because the number density of a typical species in the plasma-catalyst environment can at the same time change by surface reactions and/or plasma volume reactions. However, a general description of the conversion process by plasmas-catalyst synergy implies that methane conversion is initiated by electron impact dissociation of CH_4 to generate radicals and ions. Then the produced radicals either interact with each other in bulk plasma to form higher hydrocarbons or they are adsorbed in catalyst surface to take part in surface reactions to form again higher hydrocarbons that are released in bulk plasma by desorption processes. Heavier hydrocarbons produced in bulk plasma and by subrace reactions along with feedstock gas interact with electrons to produce new radical

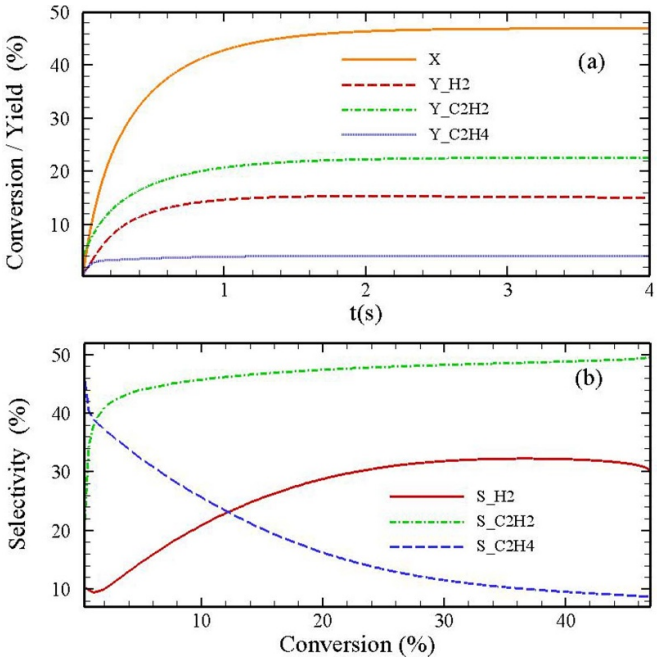

Figure 3. (a) Time evolution of methane conversion and yield of the main products of process, (b) selectivity towards the main products as a function of CH_4 conversion.

species which take part in subsequent secondary reactions. Also, in bulk plasma, the hydrocarbons interact with radicals to produce new species. This process continues until the rate of conversion reaches a steady state.

To investigate the effect of presence of catalyst inside the reactor and to see how micro kinetic surface model plays a key role in conversion result, we present figure 4 which compares the results for two processes with-catalyst and without-catalyst with each other. Figure 4(a) shows relative changes in density of species in percent when the catalyst coating is removed from inside reactor. Negative percent value implies that density of species is decreased form value that it had during process with catalyst, while positive percent value presents increase in the density. When there is no catalyst the final density of methane gas is higher, so the conversion is less for without catalyst case, which is also seen form figure 4(b). In this figure, the conversion, selectivity and yield of main species are compared for two cases with- and without-catalyst. It highlights that when catalyst is present in plasma reactor both selectivity and yield for hydrogen decrease while they increase for C_2H_2. Removing the catalyst does not significantly affect ethylene density and its selectivity and yield do not experience a big change in value. Generally, presence of catalyst inside the plasma reactor changes density of radicals, some of them are consumed by catalyst to produce heavier species while density of some other radicals increases by surface reactions. For example, density of CH_3 radical for with-catalyst case is higher than that for without-catalyst case while for CH_2 radical it is reversed. The consumption and production of radicals on catalyst surface depends overall surface processes which contains adsorption, desorption, and reactions between surface species. The surface reaction mechanism determines net flux of species

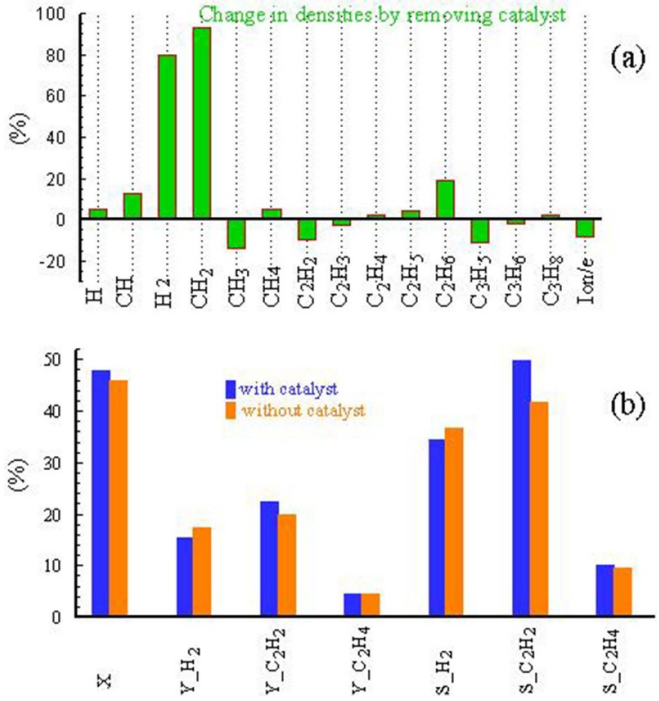

Figure 4. (a) Change in density of species by removing the catalyst (b) conversions and yield and selectivity of main species for two cases with and without catalyst.

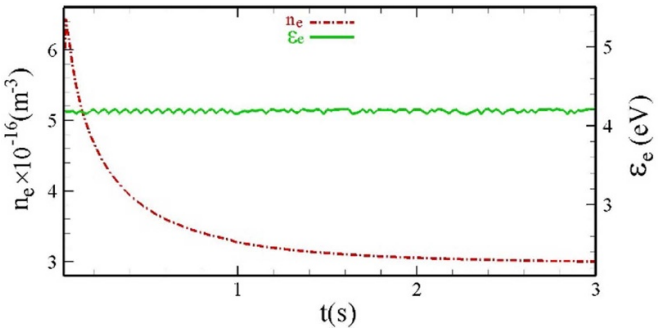

Figure 5. The electron density and energy as a function of residence time. The other conditions are the same as those in figure 2.

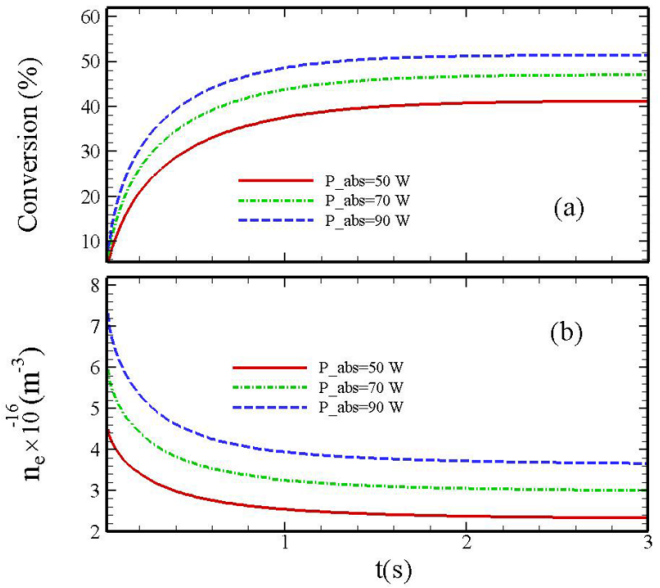

Figure 6. (a) The CH_4 conversion and (b) electron density as a function of time at discharge powers of 50, 70 and 90 W. Other parameters are same as those in figure 2.

from surface to plasma or from plasma to surface. The species that are consumed on surface their net flux direction is from plasma towards surface while net flux of species produced on surface is directed form surface towards plasma. We need to express that in atmospheric pressure plasma, densities of radicals ($n \ll 10^{19}$) are much lower than densities of background gas and produced hydrocarbons ($10^{23} \ll n$). Therefore, a big change in density of species with small density does not mean that a big change in density of species with high density must be observed. Removing catalysts from inside discharge, according to figure 4 leads to an increase in the density of H_2 and CH_2 species in the plasma phase. It means that these species are consumed in surface reactions during the catalyst presence, while the species that their density decrease by removal of catalyst are produced by surface reactions during the presence of the catalyst. Notice that figure 4(a) represents the density change of species by removing catalyst. By comparing this figure with figure 2 densities of species in the without-catalyst case can easily be estimated.

The electron density and electron energy are important parameters in NTPs that influence energy distribution between different reaction pathways. The electron energy strongly depends on the electric field distribution, which, in turn, depends on the input energy. It can be seen in figure 5 that the electron energy does not change with time as the power absorbed by discharge remains constant, which is a characteristic feature of NTPs. The electron density is determined by the ionization energy of gas molecules participating in the reactions. The electron density shows an exponential decay towards a new steady state value at 3 s (figure 5). The electron temperature in plasma depends on input power and electric field. As far as the input power is constant the electron temperature cannot change. The electron density strongly depends on ionization reactions and their rate constants. The electrons are initially produced only by ionization of CH_4, but with changing background gas due to conversion and increase in density of other hydrocarbons the rate of electron production changes. Also, according to equation (6), in constant input power and electron temperature, any change in electron density is related to energy consumed by elastic and inelastic interaction of the electron with background gas, as well as power losses to reactor walls.

Figure 6 shows the effect of discharge power on CH_4 conversion and electron density. The selectivity to the key species remains essentially the same in the whole range of applied powers studied. The CH_4 conversion and the electron density increase as the input power increases from 50 to 90 W. The conversion is directly proportional to the plasma power, reaching a maximum value at a discharge power of 90 W. This is due to the fact that the energy delivered to discharge increases the

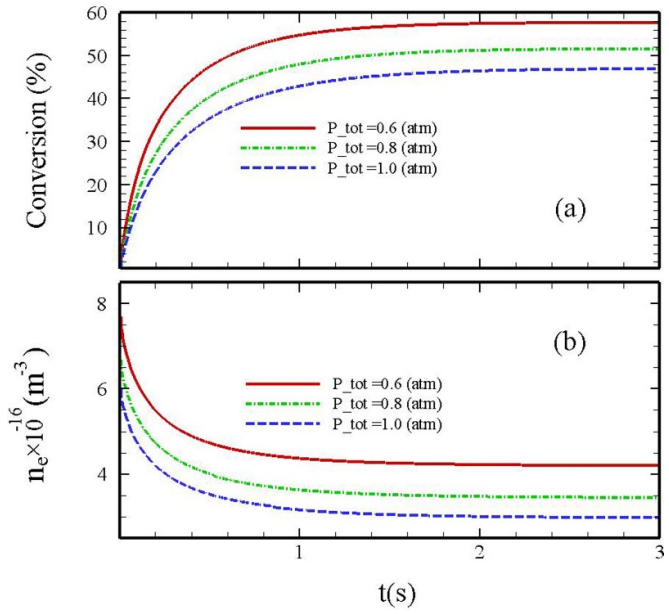

Figure 7. (a) The CH_4 conversion and (b) electron density as a function of time at pressures 0.8, 1.0 and 1.2 atm. Other parameters are same as are figure 2.

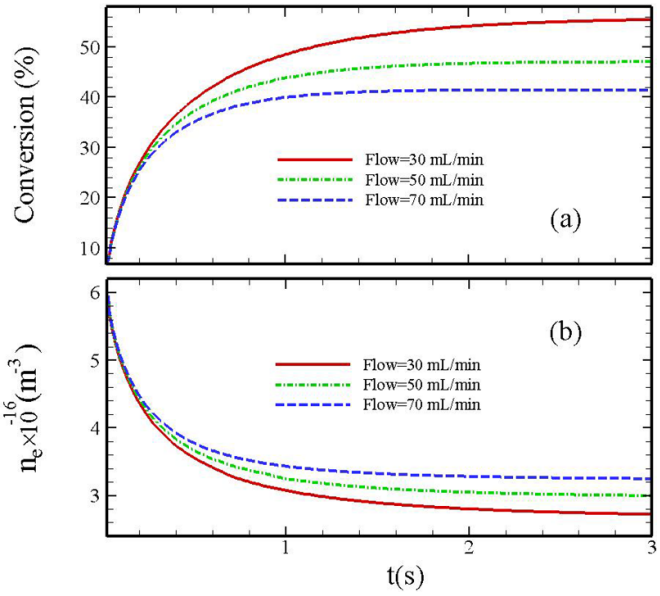

Figure 8. Time evolution of the conversion (a) and electron density (b) for three different flow rates of feedstock gas. Other parameters are same as are in figure 2.

average electron energy and electron density. In NTPs, most of the energy delivered to electrons is lost by their inelastic collisions with neutral species resulting in ionization and dissociation of CH_4 molecules. Therefore, the CH_4 conversion increases with the increase of input power. Due to the high rate of collisions in plasma, the electron energy remains rather constant, while the electron density increases with an increase in input power.

In CH_4 plasma, a considerable amount of energy is also lost by elastic collisions of the electrons with the neutral molecules in the reaction volume. Therefore, the electron density decreases with increase in pressure and the CH_4 conversion initially follows the same trend (figure 7). Increase in the electron density increases the conversion. The conversion of 51% was achieved at a pressure 0.8 atm while a higher conversion of 58% was observed at 0.6 atm. Decrease in pressure reduce the rate of momentum interaction of electron with neutral species, resulting in more ionization and dissociation processes. Increase in electron density leads to more production of radical species which have significant role in conversion process.

Finally, the last figure (figure 8) studies the effect of variation of gas flow rate on electron density and background gas conversion at constant pressure a 1 atm. At a constant pressure, which is established by adjustment in outlet flow rate, any change in inlet flow rate changes the residence time of the reactor and duration that species spends in plasma reactor before going out. Therefore, change in inlet flow rate at constant pressure corresponds with a change in residence time. As the figure shows, the electron density increases with an increase in input gas flow rate while the conversion experiences a decrease in value with an increase in gas flow rate. When the gas flow rate increases at fixed total pressure and fixed applied power the residence time of the reactor decrease and molecules of neutral species spend less time in the discharge region, as some of them leave the reactor without reacting with catalytic surface and plasma species. It results in less conversion of the background gas.

It is noteworthy to present here some validation descriptions of our model and compare our results with relevant experiment results reported in literature. A precise literature review shows that only a limited number of studies have been reported for the non-oxidative coupling of methane on the surface of transition metal catalysts in DBDs. Jo *et al* studied the effect of electric conductivity of the catalysts on methane activation in a DBD [51]. Their models revealed that alumina-supported Pt catalyst decreased electric field more significantly compared to bare alumina. The presence of a conductive metal catalyst inside the discharge zone resulted in higher CH_3 and lower CH densities. The impact of the electrode material and flow rate in discharge plasmas on the methane conversion was investigated by Spiess *et al* [52]. They showed that coated electrodes with copper and tin oxide nanoparticles exhibit high activity in comparison with other metal and copper rods. Their results also showed that the decomposition of methane and the evolution of hydrogen decreases with an increase in flow rate in a negative exponential manner due to the lower residence time. Increase in CH_3 density and decrease in CH density with presence of catalyst inside discharge region and also reduction in methane conversion by increase in flow rate in our work are in compatibility with results of above-mentioned experimental works. Therefore, they can be considered a validation for present modeling work.

4. Conclusions

A surface microkinetic model over a Cu catalyst was coupled with a volumetric plasma model to describe the performance of a NTP reactor in non-oxidative coupling of methane. The effect of residence time, pressure, and discharge power on the methane conversion and the carbon and hydrogen selectivity was investigated. The discharge power was found to be the most influential parameter for the plasma processing of methane in terms of the methane conversion and selectivity to C_2 gas products. Results showed that increase in power increases conversion while increase in pressure and/or inlet flow rate decreased in methane conversion. The selectivity of acetylene was higher than other hydrocarbon products and hydrogen molecules. The presence of Cu catalyst coating inside plasma increased the selectivity of acetylene while it decreased the selectivity of hydrogen. It also increased the conversion, although it was not high. In addition, density of radical CH_3 in plasma phase increased in the presence of catalyst, while CH_2 and CH densities decreased with that.

The model proposed in this work present a novel approach to study plasma-catalyst systems and provides an in-depth understanding from chemistry of interaction plasma with catalysts. This model can be used for any plasma-catalyst system just by changing chemistry reactions in plasma and catalyst surface. Therefore, to outlook for future works, this model can be used to study methane conversion in plasma reactors with different catalyst materials, also to investigate effect of surface temperature and modulation of it by external field on the conversion process.

Data availability statement

The data that support the findings of this study are available upon reasonable request from the authors.

Acknowledgments

The authors acknowledge support from the ERC Synergy Grant Surface-Confined fast modulated plasma for process and energy intensification (SCOPE) from the European Commission with the Grant No. 810182.

ORCID iDs

Nima Pourali https://orcid.org/0000-0002-0962-5926
Evgeny V Rebrov https://orcid.org/0000-0001-6056-9520

References

[1] Dry M E 2002 *J. Chem. Technol. Biotechnol.* **77** 43
[2] Scapinello M, Delikonstantis E and Stefanidis G D 2017 *Chem. Eng. Process.* **117** 120
[3] Horn R and Schlögl R 2015 *Catal. Lett.* **145** 23
[4] Zhang S, Gao Y, Sun H, Bai H, Wang R and Shao T 2018 *J. Phys. D: Appl. Phys.* **51** 274005
[5] Scapinello M, Delikonstantis E and Stefanidis G D 2018 *Fuel* **222** 705
[6] Delikonstantis E, Scapinello M and Stefanidis G D 2018 *Fuel Process. Technol.* **176** 33
[7] Gao Y, Zhang S, Sun H, Wang R, Tu X and Shao T 2018 *Appl. Energy* **226** 534
[8] Khalifeh O, Mosallanejad A, Taghvaei H, Rahimpour M R and Shariati A 2016 *Appl. Energy* **169** 585
[9] Lieberman M A and Ashida S 1996 *Plasma Sources Sci. Technol.* **5** 145
[10] Neyts E C, Ostrikov K, Sunkara M K and Bogaerts A 2015 *Chem. Rev.* **115** 13408–46
[11] Puliyalil H, Jurković DL, Dasireddy V D and Likozar B 2018 *RSC Adv.* **8** 27481–508
[12] Engelmann Y, Mehta P, Neyts E C, Schneider W F and Bogaerts A 2020 *ACS Sustain. Chem. Eng.* **8** 6043–54
[13] Gupta R, Gupta N and Sharma S C 2018 *Phys. Plasmas* **25** 043504
[14] Gupta R and Sharma S C 2017 *Phys. Plasmas* **24** 073504
[15] Tewari A, Ghosh S and Srivastava P 2019 *Plasma Process. Polym.* **16** 1900013
[16] Bahador H and Pourali N 2019 *Phys. Plasmas* **26** 013502
[17] Lee C and Lieberman M A 1995 *J. Vac. Sci. Technol.* A **13** 368–80
[18] Zorat R, Goss J, Boilson D and Vender D 2000 *Plasma Sources Sci. Technol.* **9** 161
[19] Liu D X, Bruggeman P, Iza F, Rong M Z and Kong M G 2010 *Plasma Sources Sci. Technol.* **19** 025018
[20] Van't Veer K, Reniers F and Bogaerts A 2020 *Plasma Sources Sci. Technol.* **29** 045020
[21] Hurlbatt A, Gibson A R, Schröter S, Bredin J, Foote A P, Grondein P, O'Connell D and Gans T 2017 *Plasma Process. Polym.* **14** 1600138
[22] Fan Q *et al* 2021 *Adv. Energy Mater.* **11** 2101424
[23] Engelmann Y, Van't Veer K, Gorbanev Y, Neyts E C, Schneider W F and Bogaerts A 2021 *ACS Sustain. Chem. Eng.* **9** 13151
[24] Hummelshøj J S, Abild-Pedersen F, Studt F, Bligaard T and Nørskov J K 2012 *Angew. Chem., Int. Ed.* **51** 272–4
[25] Carman R J and Mildren R P 2000 *J. Phys. D: Appl. Phys.* **33** L99
[26] Pourali N, Hessel V and Rebrov E V 2022 *Plasma Chem. Plasma Process.* **42** 619–40
[27] Hagelaar G J M and Pitchford L C 2005 *Plasma Sources Sci. Technol.* **14** 722
[28] De Bie C, Verheyde B, Martens T, Van Dijk J, Paulussen S and Bogaerts A 2011 *Plasma Process. Polym.* **8** 1033–58
[29] Alman D A, Ruzic D N and Brooks J N 2000 *Phys. Plasmas* **7** 1421–32
[30] Farouk T, Farouk B, Gutsol A and Fridman A 2008 *J. Phys. D: Appl. Phys.* **41** 175202
[31] Janev R K and Reiter D 2002 *Phys. Plasmas* **9** 4071–81
[32] Janev R K and Reiter D 2004 *Phys. Plasmas* **11** 780–829
[33] Mao M and Bogaerts A 2010 *J. Phys. D: Appl. Phys.* **43** 205201
[34] Jeong J, Hwang A, kim Y T, Hong D-Y and Park M-J 2020 *Catal. Today* **352** 140–7
[35] Pourali N, Sarafraz M M, Hessel V and Rebrov E V 2021 *Phys. Plasmas* **28** 013502
[36] Nienhuis G J, Goedheer W J, Hamers E A, van Sark W G and Bezemer J 1997 *J. Appl. Phys.* **82** 2060–71
[37] Lallement L, Rhallabi A, Cardinaud C, Peignon-Fernandez M C and Alves L L 2009 *Plasma Sources Sci. Technol.* **18** 025001
[38] Park G, Lee H, Kim G and Lee J K 2008 *Plasma Process. Polym.* **5** 569–76
[39] Nam S K and Verboncoeur J P 2009 *Comput. Phys. Commun.* **180** 628–35

[40] Lieberman M A and Lichtenberg A J 2005 *Principles of Plasma Discharges and Materials Processing* (New York: Wiley)
[41] Ferrin P, Kandoi S, Nilekar A U and Mavrikakis M 2012 *Surf. Sci.* **606** 679–89
[42] Kulkarni A R, Zhao Z-J, Siahrostami S, Nørskov J K and Studt F 2016 *ACS Catal.* **6** 6531–6
[43] Wang S *et al* 2011 *Phys. Chem. Chem. Phys.* **13** 20760–5
[44] Vojvodic A *et al* 2011 *J. Chem. Phys.* **134** 244509
[45] Wittreich G R, Alexopoulos K and Vlachos D G 2018 Microkinetic modeling of surface catalysis *Handbook of Materials Modeling* (Berlin: Springer) pp 1377–404
[46] Johnson R D III 2013 NIST computational chemistry comparison and benchmark database *Release 16a* (available at: http://cccbdb.nist.gov/) (Accessed 13 March 2015)
[47] Díaz C, Pijper E, Olsen R A, Busnengo H F, Auerbach D J and Kroes G J 2009 *Science* **326** 832–4
[48] Zhao B, Zhang R, Huang Z and Wang B 2017 *Appl. Catal.* A **546** 111–21
[49] Monahan D D and Turner M M 2008 *Plasma Sources Sci. Technol.* **17** 045003
[50] Gudmundsson J T 2002 *J. Phys. D: Appl. Phys.* **35** 328
[51] Jo S, Kim T, Lee D H, Kang W S and Song Y-H 2014 *Plasma Chem. Plasma Process.* **34** 175–86
[52] Spiess F-J, Suib S L, Irie K, Hayashi Y and Matsumoto H 2004 *Catal. Today* **89** 35–45